Comparing the dynamical effects of symmetric and antisymmetric stretch excitation of methane in the $Cl+CH_4$ reaction

Hans A. Bechtel, Jon P. Camden, Davida J. Ankeny Brown, and Richard N. Zare[a)]
Department of Chemistry, Stanford University, Stanford, California 94305-5080

(Received 2 December 2003; accepted 18 December 2003)

The effects of two nearly isoenergetic C–H stretching motions on the gas-phase reaction of atomic chlorine with methane are examined. First, a 1:4:9 mixture of Cl_2, CH_4, and He is coexpanded into a vacuum chamber. Then, either the antisymmetric stretch ($\nu_3=3019\ cm^{-1}$) of CH_4 is prepared by direct infrared absorption or the infrared-inactive symmetric stretch ($\nu_1=2917\ cm^{-1}$) of CH_4 is prepared by stimulated Raman pumping. Photolysis of Cl_2 at 355 nm generates fast Cl atoms that initiate the reaction with a collision energy of $1290\pm175\ cm^{-1}$ (0.16 ± 0.02 eV). Finally, the nascent HCl or CH_3 products are detected state-specifically via resonance enhanced multiphoton ionization and separated by mass in a time-of-flight spectrometer. We find that the rovibrational distributions and state-selected differential cross sections of the HCl and CH_3 products from the two vibrationally excited reactions are nearly indistinguishable. Although Yoon *et al.* [J. Chem. Phys. **119**, 9568 (2003)] report that the reactivities of these two different types of vibrational excitation are quite different, the present results indicate that the reactions of symmetric-stretch excited or antisymmetric-stretch excited methane with atomic chlorine follow closely related product pathways. Approximately 37% of the reaction products are formed in $HCl(v=1,J)$ states with little rotational excitation. At low J states these products are sharply forward scattered, but become almost equally forward and backward scattered at higher J states. The remaining reaction products are formed in $HCl(v=0,J)$ and have more rotational excitation. The $HCl(v=0,J)$ products are predominantly back and side scattered. Measurements of the CH_3 products indicate production of a non-negligible amount of umbrella bend excited methyl radicals primarily in coincidence with the $HCl(v=0,J)$ products. The data are consistent with a model in which the impact parameter governs the scattering dynamics. © *2004 American Institute of Physics.* [DOI: 10.1063/1.1647533]

I. INTRODUCTION

Experimental and theoretical work has shown that reagent vibrational excitation can have dramatic effects on chemical reactions. One of the most obvious effects of vibrational excitation is an increase in reactivity. Indeed, Polanyi[1] found that vibrational excitation is more efficient than translational energy in promoting endoergic atom plus diatom reactions with late reaction barriers. For systems involving polyatomic reagents, the extra degrees of freedom associated with polyatomics can complicate this simple picture and lead to a large number of different vibrational motions. Several groups[2–16] have demonstrated that excitation of certain vibrational motions can localize energy in specific parts of the polyatomic reagent and lead to dramatic bond- and mode-selectivity.[17–19] The first examples of such behavior involved reactions of fast H atoms with various isotopes of water.[2,3] This method of vibrational control has recently been extended to larger systems, such as the reaction of methane with atomic chlorine[13,14,16] or nickel surfaces.[15]

Although most of these bond- and mode-selective studies have focused on the effects of rather different vibrational motions, the effects of seemingly similar motions on chemical reactivity is also of particular interest. In 1979, Schatz[20] used quasiclassical trajectory calculations to determine that the symmetric stretch of a linear triatomic molecule is more efficient at promoting reaction than a comparable amount of excitation in the antisymmetric stretch. Since then, a variety of theoretical methods have been used to examine the relative reactivity of the symmetric and antisymmetric stretches in a number of polyatomic reaction systems.[21–31] Palma and Clary[29] performed four-dimensional quantum scattering calculations on the $O(^3P)+CH_4\rightarrow OH+CH_3$ system and found the symmetric stretch of CH_4 to be more reactive than the antisymmetric stretch. Fair *et al.*[32] found similar results with wave packet calculations on the $Cl+H_2O\rightarrow HCl+OH$ reaction: the symmetric stretch of H_2O is more reactive than the antisymmetric stretch. They attributed the increased reactivity to the adiabatic flow of vibrational energy into local-mode OH excitations pointing either toward (proximal) or away (distal) from the approaching Cl atom for the symmetric and antisymmetric stretches of H_2O, respectively.

Despite numerous theoretical studies, few experimental investigations have compared the effects of the symmetric and antisymmetric stretches on chemical reactions. Yoon *et al.*[33] examined the relative reactivity of the stretch–bend combination vibrations of CH_4 in the $Cl+CH_4\rightarrow HCl+CH_3$ reaction using infrared excitation and action spectroscopy. They found the symmetric stretch–bend combination ($\nu_1+\nu_4$) more reactive than the antisymmetric stretch–bend

a)Author to whom all correspondence should be addressed; electronic mail: zare@stanford.edu

combination ($\nu_3+\nu_4$) by a factor of 1.9 ± 0.5. Direct comparisons of the symmetric and antisymmetric stretch, however, could not be made because the symmetric stretch (ν_1) of CH_4 is infrared inactive and the effects of the bending mode (ν_4) on the reaction are not known. Recently, Yoon *et al.*[34] exploited the reduced symmetry of CH_3D, which makes both the symmetric and antisymmetric stretches infrared active. They found that the symmetric stretch is seven times more reactive than the antisymmetric stretch in the $Cl+CH_3D\rightarrow HCl+CH_2D$ reaction.

The large difference in reactivity between these two seemingly similar C–H stretching motions is surprising, especially considering that both C–H stretches are expected to map effectively onto the reaction coordinate. Indeed, we might expect the antisymmetric stretch to be more reactive than the symmetric stretch because some of the C–H bonds in the antisymmetric stretch extend more than the bonds in the symmetric stretch.[35] Clearly, the dynamics of vibrationally excited reactions are more complicated than this simple picture, which appears to be invalidated by the predicted and measured increased reactivity of the symmetric stretch over the antisymmetric stretch. The large difference in reactivity raises the possibility that these two vibrationally excited reactions proceed via different mechanisms. The present study contradicts this supposition in part. Instead, we suggest that the reactions of these two differently prepared vibrationally excited reagents must follow a similar pathway leading to product formation. Thus, it is possible that the initial preparation of the reagents affects the reactivity, but not the dynamics of the reaction.

Here, we use the *photoloc* technique to examine the effects of the symmetric (ν_1) and antisymmetric (ν_3) stretches on the dynamics of the $Cl+CH_4\rightarrow HCl+CH_3$ reaction. Simpson *et al.*[36] previously used the same technique to examine the $Cl+CH_4(\nu_3)$ reaction with an unprecedented level of detail, obtaining rotational distributions, state-selected differential cross sections (DCSs), and information on the effects of rotational and vibrational alignment on chemical reactivity. These measured quantities have recently been used to differentiate the effects of two nearly isoenergetic vibrations on the $Cl+CH_2D_2$ reaction[16] and are known be sensitive probes of chemical dynamics. We use stimulated Raman pumping (SRP) to excite the fundamental of the symmetric stretch (ν_1) and infrared excitation to excite the fundamental of the triply degenerate antisymmetric stretch (ν_3). To reduce any systematic errors, both reactions were performed under identical conditions. We find the repeated measurements of the $Cl+CH_4(\nu_3)$ reaction to be in excellent agreement with previous measurements.[36]

II. ENERGETICS AND EXPERIMENTAL PROCEDURES

Figure 1 displays the relevant energetics of the $Cl+CH_4\rightarrow HCl+CH_3$ reaction. The reaction is slightly endothermic,[37] $\Delta H=600\ cm^{-1}$ (1.7 kcal/mol), and has an activation barrier in the 800–1300 cm^{-1} (2.4–3.6 kcal/mol) or 1300–1900 cm^{-1} (3.6–5.5 kcal/mol) range, based on experimental[38] or *ab initio* calculations,[28] respectively. The combination of translational and vibrational energy is used to overcome the reaction barrier. Photolysis of Cl_2 at 355 nm provides $1290\pm175\ cm^{-1}$ of translational energy in the center of mass frame. Excitation of the symmetric stretch (ν_1) provides 2917 cm^{-1} of vibrational energy, whereas excitation of the antisymmetric stretch (ν_3) provides 3019 cm^{-1} of vibrational energy.

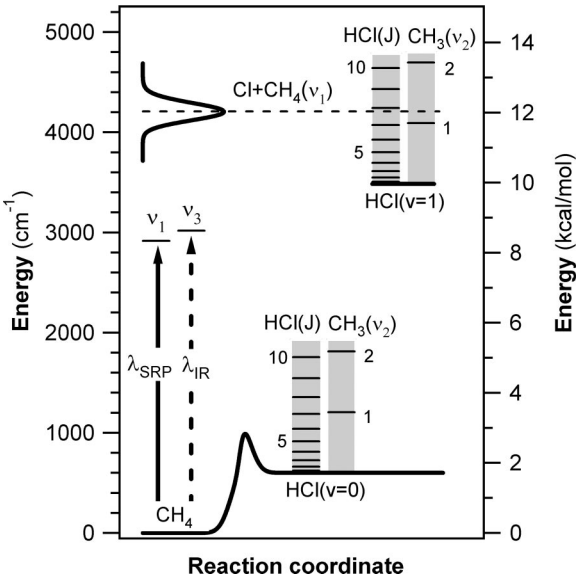

FIG. 1. Energy level diagram for the reaction of atomic chlorine with vibrationally excited methane. The symmetric stretch ($\nu_1=2917\ cm^{-1}$) is prepared by stimulated Raman pumping (SRP) and the antisymmetric stretch ($\nu_3=3019\ cm^{-1}$) is prepared by direct infrared absorption (IR). Photolysis of Cl_2 at 355 nm provides 1290 cm^{-1} of collision energy with an energy spread determined from the formulas of van der Zande *et al.* (Ref. 54) at 15 K.

The methods and experimental apparatus have been described in detail previously,[36,39] therefore, only the primary features are presented here. A 1:4:9 mixture of molecular chlorine (Matheson, research grade, 99.999%), methane (Matheson, 99.999%), and helium (Liquid Carbonic, 99.995%) is supersonically expanded into the extraction region of a linear time-of-flight (TOF) spectrometer having a Wiley-McLaren configuration.[40] The vibrational state of CH_4 is prepared by SRP (ν_1) or direct IR excitation (ν_3). The reaction is initiated by the photolysis of Cl_2 with linearly polarized 355 nm light, which produces monoenergetic Cl atoms primarily in the ground state ($^2P_{3/2}$) with an anisotropy parameter $\beta=-1$.[41] After a 20–80 ns time delay, the HCl or CH_3 products are state selectively ionized by $2+1$ resonance-enhanced multiphoton ionization (REMPI), separated by mass, and detected by microchannel plates. The reactive signal from vibrationally excited methane is separated from backgrounds by modulating the SRP or IR light and subtracting the resultant signals on a shot-by-shot basis.

The SRP radiation required to excite the symmetric stretch (ν_1) of CH_4 is generated by a Nd^{3+}:YAG laser (Continuum PL8020) and a pulsed dye laser (Quanta-Ray, PDL-3). Although the Nd^{3+}:YAG second harmonic (532 nm) is more commonly used as the pump source for SRP, we found that the 532 nm light excited the Cl_2 precursor, resulting in large ion backgrounds that interfere with the reaction signal. To avoid these backgrounds, we use the output of the dye laser (Exciton LDS 821) to generate ~812 nm light (λ_{pump})

and the fundamental from the Nd^{3+}:YAG laser to generate 1064 nm light (λ_{Stokes}). The 1064 nm light is combined collinearly with the 812 nm light using an 800 nm high reflector. In order to find the frequency condition between the pump and Stokes lasers, a photodiode is used to detect the coherent anti-Stokes Raman (CARS) signal at ~657 nm which is generated in a separate cell containing ~20 Torr of CH_4. The CARS spectrum consists of only *Q*-branch transitions because the ν_1 vibration is the totally symmetric C–H stretch. The resolution of our dye laser (~0.1 cm^{-1}) proved to be insufficient to fully resolve individual *Q*-branch members. Typical laser energies of the 812 and 1064 nm light are ~25 and 200 mJ, respectively. The pump and Stokes beams are focused into the chamber with an $f=45$ cm CaF_2 lens.

The IR radiation required to excite the antisymmetric stretch (ν_3) of CH_4 is generated in a two-step process involving difference-frequency mixing and optical parametric amplification. First, mid-IR light at $\lambda=3.3$ μm is generated via difference-frequency mixing by combining the 1064 nm fundamental of an Nd^{3+}:YAG laser (Continuum PL9020) with the ~804 nm output of a dye laser (Continuum ND6000, Exciton LDS 821) in a lithium niobate ($LiNbO_3$) crystal. The mid-IR radiation is then parametrically amplified in a second $LiNBO_3$ crystal pumped by another 1064 nm beam to produce approximately 10 mJ of the requisite light. The frequency condition of the IR light is found by using a photoacoustic cell containing ~10 Torr of CH_4. Once the reaction signal is found, care is taken to attenuate and defocus the IR light to avoid two-photon absorption to the first overtone of the antisymmetric stretch ($2\nu_3$), which produces stretch-excited methyl radical. The ν_3 vibrational state is prepared on the *Q*-branch bandhead or on single *R*-branch lines. With the exception of a slight increase in forward scattered behavior for HCl($v=1$) products,[36] the data show no strong dependence on the CH_4 rotational state.

The photolysis light is generated from the third harmonic of a Nd^{3+}:YAG laser (Continuum PL9020), and the probe light for REMPI is generated by frequency doubling the fundamental of a dye laser output (Quanta Ray DCR-2A, Lambda Physik FL 2002, Exciton LD489 or DCM/LDS698) in a BBO crystal. The HCl products are detected via the $f\,^3\Delta_2-X\,^1\Sigma^+(0,0)$, $F\,^1\Delta_2-X\,^1\Sigma^+(0,0)$, $F\,^1\Delta_2-X\,^1\Sigma^+(1,1)$, and the $E\,^1\Sigma^+-X\,^1\Sigma^+(0,1)$ bands.[42,43] The methyl radical products are detected by the $3p_z\,^2A_2''-X\,^2B_1''$ band.[44] Approximately 2 mJ of ~240 nm light is used to probe the HCl products, and less than 1.5 mJ of ~330 nm light is used to probe the CH_3 products. The probe light is focused into the chamber using a $f=50$ cm fused-silica lens.

A photoelastic modulator (PEM-80, Hinds International Inc.) flips the direction of the photolysis laser polarization between parallel and perpendicular to the TOF axis on an every-other-shot basis in order to obtain the isotropic $\mathbf{I}_{iso}=\mathbf{I}_{\parallel}+2\mathbf{I}_{\perp}$ and anisotropic $\mathbf{I}_{aniso}=2(\mathbf{I}_{\parallel}-\mathbf{I}_{\perp})$ components of the core-extracted TOF profiles. The isotropic TOF profile removes any dependence on the photolysis spatial anisotropy and thus provides a direct measurement of the speed distribution. These profiles are analyzed and converted into DCSs by a method similar to that of Simpson *et al.*[36] The anisotropic TOF profiles are analyzed to estimate the amount of internal energy deposited into the co-product by a method described in previous publications.[39,45]

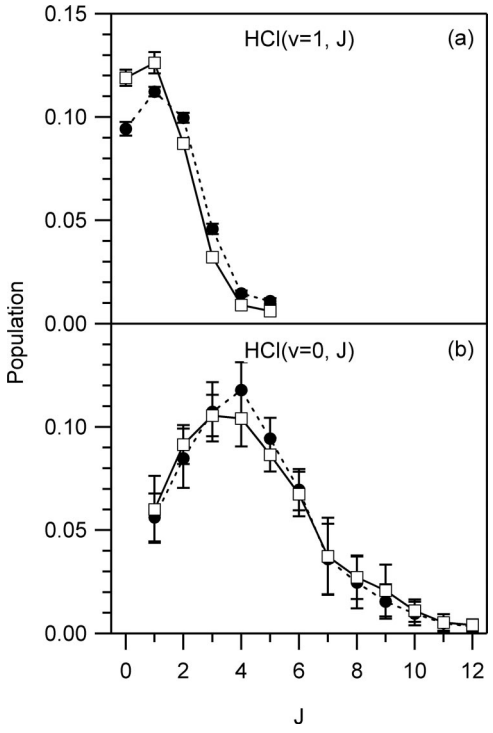

FIG. 2. Rotational distributions of the (a) HCl($v=1,J$) and (b) HCl($v=0,J$) products from the reaction of atomic chlorine with vibrationally excited methane. The HCl(v,J) populations from the $Cl+CH_4(\nu_1)$ reaction are represented by open squares and solid lines, and the HCl(v,J) populations from the $Cl+CH_4(\nu_3)$ reaction are represented by closed circles and dotted lines. The HCl($v=0,J$) and HCl($v=1,J$) populations are scaled relative to one another. The error bars represent 95% confidence intervals of replicate measurements.

III. RESULTS

A. HCl product state distributions

For the $Cl+CH_4(\nu_1)$ and $Cl+CH_4(\nu_3)$ reactions Figs. 2(a) and 2(b) present the integral cross sections for HCl($v=1,J$) and HCl($v=0,J$), respectively. The HCl($v=0,J$) populations are obtained by detecting the $m/z=36$ ($H^{35}Cl^+$) ion signal while scanning the probe laser over the *Q*, *R*, and *S* branches of the $F\,^1\Delta_2-X\,^1\Sigma^+(0,0)$ 2+1 REMPI band and the *Q* branch of the $f\,^3\Delta_2-X\,^1\Sigma^+(0,0)$ 2+1 REMPI band. Signal intensities are converted into relative populations using empirical correction factors determined by leaking room temperature HCl into the vacuum chamber. The HCl($v=1,J$) populations are obtained by detecting the $m/z=1$ (H^+) ion signal from dissociative ionization of HCl while scanning the probe laser over the *Q* branch of the $E\,^1\Sigma^+-X\,^1\Sigma^+(0,1)$ 2+1 REMPI band. The correction factors of Simpson *et al.*[36] are used to convert the HCl($v=1$) signal intensity to population. The HCl($v=0,J$) and HCl($v=1,J$) rotational distributions are scaled with respect to each other by recording the intensity of the $R(1)$ member of the $F\,^1\Delta_2-X\,^1\Sigma^+(1,1)$ 2+1 REMPI band in the same scan as the $R(5)$ member of the $F\,^1\Delta_2-X\,^1\Sigma^+(0,0)$ 2+1 REMPI

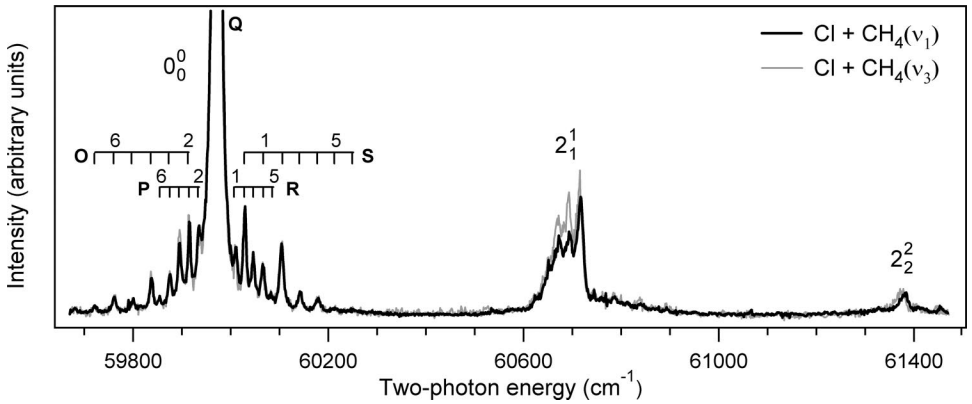

FIG. 3. Co-added 2+1 REMPI spectra of the CH_3 products from the Cl+$CH_4(\nu_1)$ reaction, black line, and the Cl+$CH_4(\nu_3)$ reaction, gray line. The *Q* branch of the 0_0^0 band is presented off scale in order to see the rotational structure of the *O*, *P*, *R*, and *S* branches. The integrated intensity ratio of the 0_0^0, 2_1^1, and 2_2^2 bands for the Cl+$CH_4(\nu_1)$ reaction is 0.80 ± 0.03:0.18 ± 0.02:0.02 ± 0.01. The integrated intensity ratio of the three bands for the Cl+$CH_4(\nu_3)$ reaction is 0.76 ± 0.02:0.21 ± 0.02:0.03 ± 0.01. The errors represent 95% confidence intervals of replicate measurements.

band. The vibrational correction factor for the relative sensitivity of the diagonal bands of the $F\,^1\Delta_2-X\,^1\Sigma^+$ band is obtained by tuning the IR laser to various HCl rovibrational lines and scanning the probe laser over the depleted $F\,^1\Delta_2-X\,^1\Sigma^+(0,0)$ lines and the enhanced $F\,^1\Delta_2-X\,^1\Sigma^+(1,1)$ lines. Every effort was made to ensure that the probe laser power and focusing conditions were identical for the measurement of the HCl(v,J) integral cross sections from the Cl+$CH_4(\nu_1)$ and the Cl+$CH_4(\nu_3)$ reactions. The uncertainties represent 95% confidence intervals of replicate measurements and include the error in the determination of the correction factors.

As shown in Fig. 2, the HCl integral state distributions for the Cl+$CH_4(\nu_1)$ and the Cl+$CH_4(\nu_3)$ reactions are nearly identical. For both reactions, $37\pm7\%$ of the reaction products are formed in HCl($v=1,J$) states. The average energy in rotation for the HCl($v=1$) products is 41 ± 3 and $53\pm3\ \mathrm{cm}^{-1}$, and the average energy in rotation for the HCl($v=0$) products is 301 ± 95 and $292\pm93\ \mathrm{cm}^{-1}$ for the Cl+$CH_4(\nu_1)$ and the Cl+$CH_4(\nu_3)$ reactions, respectively. Accounting for the $\sim100\ \mathrm{cm}^{-1}$ difference in the vibrational frequencies of the two C–H stretches, the average energy in rotation for the HCl($v=1$) products is only ~6% of the available energy for both the Cl+$CH_4(\nu_1)$ and the Cl+$CH_4(\nu_3)$ reactions. Although the HCl($v=0$) rotational distributions are much warmer than the HCl($v=1$) rotational distributions, the average energy in rotation is still only a small fraction of the available energy: ~8% for both reactions.

B. CH_3 product state distributions

Figure 3 displays the 2+1 REMPI spectra of the CH_3 products from the Cl+$CH_4(\nu_1)$ and Cl+$CH_4(\nu_3)$ reactions obtained with linearly polarized light. The *Q* branch of the 0_0^0 band is presented off-scale in order to display the rotational structure of the *O, P, R*, and *S* branches and the progression of bands resulting from umbrella bend excitation (2_1^1 and 2_2^2 bands). Obtaining rovibrational state distributions from the $3p_z\,^2A_2''-X\,^2B_1''$ REMPI scheme is nontrivial because the Franck–Condon factors are unknown and substantial predissociation occurs in the upper electronic state. Although attempts have been made to quantify these values,[46,47] we choose instead to make only qualitative comparisons of the CH_3 product REMPI spectra from the Cl+$CH_4(\nu_1)$ and Cl+$CH_4(\nu_3)$ reactions.

Figure 3 clearly shows that the CH_3 product-state distribution of the Cl+$CH_4(\nu_1)$ reaction is similar to the CH_3 product-state distribution of the Cl+$CH_4(\nu_3)$ reaction. The rotational structure of the two reactions in the 0_0^0 band region appears indistinguishable, indicating that the ground state methyl radical products have essentially identical rotational distributions. Both rotational distributions have no observable population in states higher than $N=7$. Moreover, both spectra show that the *O* and *S* branches are enhanced over the *P* and *R* branches. There also appears to be an enhancement of the even lines over the odd lines for the *O* and *S* branches. The enhancement of the *O* and *S* branches and the alternating intensities suggest that the methyl radical products are formed preferentially in low *K* states,[46] indicating that the methyl radical is rotating about a C_2 axis that passes through a C–H bond rather than rotating about the C_3 axis that passes through the C atom perpendicular to the plane of the molecule.

Both reactions produce non-negligible amounts of umbrella bend excited methyl radical. The integrated intensity ratio of the 0_0^0, 2_1^1, and 2_2^2 bands for the Cl+$CH_4(\nu_1)$ reaction is 0.80 ± 0.03:0.18 ± 0.02:0.02 ± 0.01, whereas the integrated intensity ratio of the three bands for the Cl+$CH_4(\nu_3)$ reaction is 0.76 ± 0.02:0.21 ± 0.02:0.03 ± 0.01. The uncertainties given represent 95% confidence intervals of replicate measurements. Yoon *et al.*[34] observed a similar ratio of ground state to umbrella bend excited CHD_2 products in the reaction of Cl+CHD_3 (ν_1 or ν_4). Although it is possible that the Cl+$CH_4(\nu_3)$ reaction generates more umbrella bend excited methyl radical products than the Cl+$CH_4(\nu_1)$ reaction, the difference is not discernible within our uncertainty.

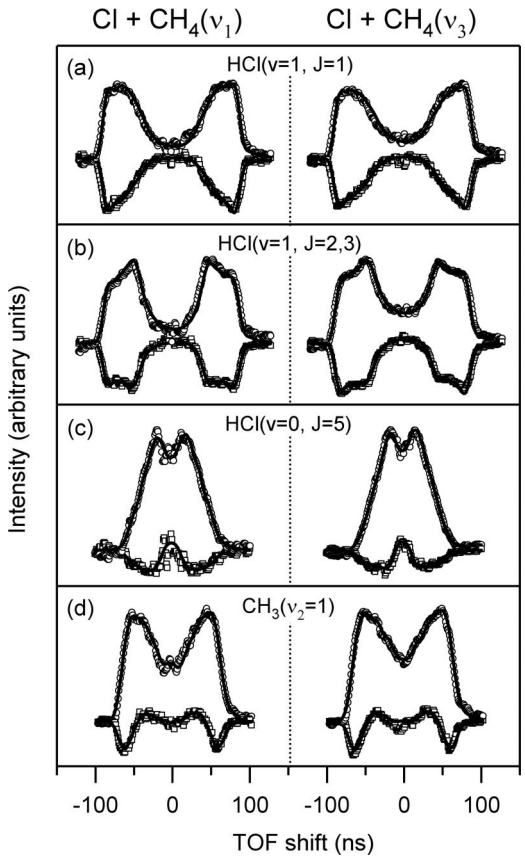

FIG. 4. Isotropic $I_{iso}=I_{\parallel}+2I_{\perp}$ and anisotropic $I_{aniso}=2(I_{\parallel}-I_{\perp})$ components of the core-extracted TOF profiles of the (a) HCl($v=1,J=1$) products, (b) the HCl($v=1,J=2,3$) products, (c) the HCl($v=0,J=5$) products, and (d) the $CH_3(\nu_2=1)$ products from the reaction of atomic chlorine with vibrationally excited methane. The profiles in the left-hand column are from the $Cl+CH_4(\nu_1)$ reaction, and the profiles in the right-hand column are from the $Cl+CH_4(\nu_3)$ reaction. The open circles are the measured isotropic TOF profiles, the open squares are the measured anisotropic TOF profiles, and the solid lines are the results of the fit.

C. State-to-state scattering distributions

Figure 4 shows the isotropic $I_{iso}=I_{\parallel}+2I_{\perp}$ and anisotropic $I_{aniso}=2(I_{\parallel}-I_{\perp})$ core-extracted TOF profiles of the HCl($v=1,J=1$), HCl($v=1,J=2,3$), HCl($v=0,J=5$), and $CH_3(\upsilon_2=1)$ products from the $Cl+CH_4(\nu_1)$ and $Cl+CH_4(\nu_3)$ reactions. The HCl($v=1,J=1$) TOF profiles are obtained on the $R(1)$ line of the $F\,^1\Delta_2-X\,^1\Sigma^+(1,1)$ band; the HCl($v=1,J=2,3$) TOF profiles are obtained on the overlapped $Q(2)$ and $Q(3)$ lines of the $F\,^1\Delta_2-X\,^1\Sigma^+(1,1)$ transition; the HCl($v=0,J=5$) TOF profiles are obtained on the $Q(5)$ line of the $f\,^3\Delta_2-X\,^1\Sigma^+(1,1)$ band; and the $CH_3(\nu_2=1)$ TOF profiles are obtained on the Q branch of the 2_1^1 band of the $3p_z\,^2A_2''-X\,^2B_1''$ band. Accurate $CH_3(\nu=0)$ TOFs could not be obtained because the transfer of population to the C–H stretching states in CH_4 necessarily depletes the signal arising from the reaction of Cl with ground-state CH_4. The ground-state reaction does not produce $CH_3(\nu_2=1)$, however, and thus we could obtain $CH_3(\nu_2=1)$ TOF profiles. The TOF profiles have a clear dependence on product state; but for each product state, the TOF profiles from the $Cl+CH_4(\nu_1)$ reaction are nearly indistinguishable from the TOF profiles of the $Cl+CH_4(\nu_3)$ reaction.

The isotropic TOF profile is a measurement of the velocity distribution of the products. Under perfect core-extraction conditions, there is a one-to-one relationship between the TOF shift and the velocity of the product ions in the lab frame. Thus, large positive TOF shifts correspond to fast products moving initially toward the detector, and large negative TOF shifts correspond to fast products moving initially away from the detector. The distribution of product lab-frame speeds can be extracted by fitting the isotropic TOF profile with a set of basis functions generated by Monte Carlo simulation, as described in a previous publication.[39] These speed distributions can be converted into DCSs with knowledge of the internal energy of the co-product state. We obtain this information by fitting the anisotropic TOF profile, which is a measurement of the product speed-dependent spatial anisotropy and provides a means of determining the average internal energy deposited in the co-product.[39]

Unfortunately, the kinematics of the HCl($v=1,J$) products constrain the measurable spatial anisotropy such that it is of little aid in determining the energy deposited in the methyl fragment. Because most of the HCl($v=1,J$) product intensity occurs outside the allowed speed range for products that are generated in coincidence with umbrella bend excited methyl radical, we assume that the methyl radical consumes no energy and all the excess is present in translation. Moreover, the spatial anisotropy of the $CH_3(\nu_2=1)$ product shows that minimal energy is deposited into the HCl co-products, indicating that the formation of HCl($v=1,J$) products in coincidence with $CH_3(\nu_2=1)$ products is a minor channel. We assume that the $CH_3(\nu_2=1)$ products are formed entirely with HCl($v=0,J$) products and that the HCl($v=0,J$) co-products have the same rotational distribution as shown earlier. The spatial anisotropy of the HCl($v=0,J=5$) products also indicates that minimal energy is deposited into the methyl radical. We are unable to differentiate between HCl($v=0,J=5$) products formed in coincidence with methyl radical in the ground state or umbrella bend excited, but the DCS associated with each co-product state is the same within our error bars.

Figure 5 shows the resulting DCSs of the different product states from both the $Cl+CH_4(\nu_1)$ and the $Cl+CH_4(\nu_3)$ reactions. As suggested by the TOF profiles, the scattering distributions for each product state are nearly identical for both reactions. The HCl($v=1,J=1$) DCSs are both sharply peaked in the forward scattered region. The HCl($v=1,J=2,3$) DCSs are also peaked in the forward scattered region, but have more intensity in the backward scattered region than the HCl($v=1,J=1$) DCSs. The HCl($v=0,J=5$) products are predominantly backward and side scattered, whereas the $CH_3(\nu_2=1)$ products are predominantly forward and side scattered.

IV. DISCUSSION

As shown in Figs. 2–5, the rovibrational distributions and scattering distributions of the products from the $Cl+CH_4(\nu_1)$ and $Cl+CH_4(\nu_3)$ reactions are nearly indistinguishable. In fact, the only difference discernable within our signal to noise and resolution is a slightly warmer HCl($v=1$) rotational distribution for the $Cl+CH_4(\nu_3)$ reaction.

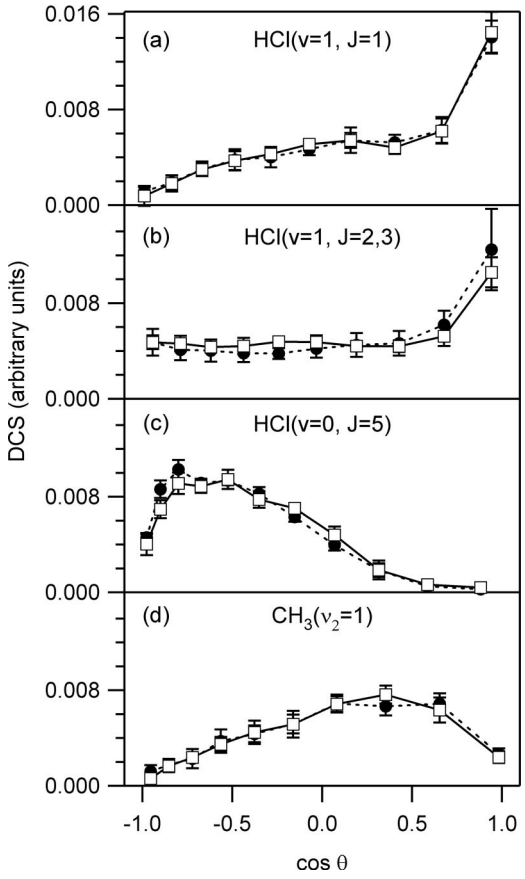

FIG. 5. State-to-state differential cross sections for the (a) HCl($v=1,J=1$) products, (b) the HCl($v=1,J=2,3$) products, (c) the HCl($v=0,J=5$) products, and (d) the $CH_3(\nu_2=1)$ products from the reaction of atomic chlorine with vibrationally excited methane. The DCSs of the products from the Cl+$CH_4(\nu_1)$ reaction are represented by open squares and solid lines, and the DCSs of the products from the Cl+$CH_4(\nu_3)$ reaction are represented by closed circles and dotted lines. The error bars represent 95% confidence intervals of replicate measurements.

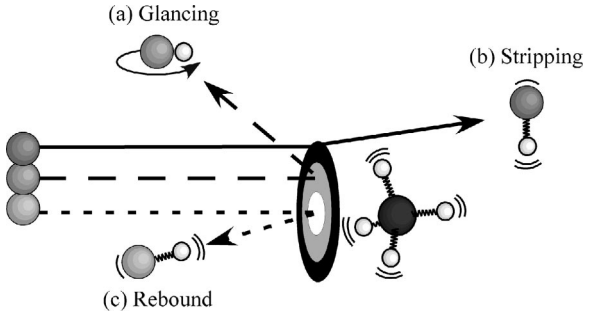

FIG. 6. Schematic model of the observed scattering behavior from the Cl+$CH_4(\nu_1)$ reaction and the Cl+$CH_4(\nu_3)$ reaction. The HCl($v=0,J$) products result from (a) glancing collisions that cause side-scattering and rotational excitation. The HCl($v=1,J$) products are formed via two competing mechanisms: (b) stripping and (c) rebound. The stripping mechanism leads to forward-scattered HCl($v=1,J$) products with little rotational excitation, and the rebound mechanism leads to backward-scattered HCl($v=1,J$) products that have more rotational excitation.

Because the HCl($v=1,J$) products are close to the energetic limit of the reaction, they are more likely to be sensitive to small differences in the reaction energetics. Consequently, the difference in the HCl($v=1$) rotational distribution simply may arise from the extra $\sim$100 cm^{-1} in the antisymmetric stretch (ν_3). The remaining rovibrational distributions and scattering distributions, however, are identical within our signal-to-noise ratio, from which we conclude that the reactive mechanisms of the two reactions are the same.

Simpson *et al.*[36] proposed a model for the Cl+$CH_4(\nu_3)$ reaction in which the impact parameter determines where the products are scattered and how the energy is partitioned between vibrational, rotational, and translational energy. Based on the results shown above, we believe the same model explains the rovibrational and scattering distributions of the Cl+$CH_4(\nu_1)$ reaction. Figure 6 illustrates the different mechanisms present in the reaction of atomic chlorine with vibrationally excited methane. Because the HCl($v=1,J$) DCS changes as the rotational number is increased, we believe there are two competing mechanisms that form HCl($v=1,J$) products. The dominant mechanism corresponds to the reaction of Cl with a peripheral H atom, resulting in forward scattered HCl($v=1$) products. This ''stripping'' mechanism imparts little torque on the HCl($v=1$) products, and consequently leaves them rotationally cold. The other mechanism arises from collisions at low-impact parameter causing the HCl($v=1$) products to ''rebound'' in the backscattered direction. The impulse release associated with the redirection of the Cl initial velocity should cause these backscattered products to be more rotationally excited. Indeed, this behavior is exactly what we observe. The low J HCl($v=1$) products are sharply forward scattered, whereas the higher J HCl($v=1$) products are more equally forward and back scattered. The steric measurements of Simpson *et al.*[36] further support the proposed ''stripping'' mechanism by showing that the forward scattered behavior of the HCl($v=1,J=1$) products results from T-shaped transition state geometries.

The observed HCl($v=0,J$) products are rotationally excited and predominantly back and side scattered. The CH_3 REMPI spectrum and the measured spatial anisotropy show that little internal energy is deposited into the methyl fragment, with only the umbrella excited bending mode significantly excited. Because little energy is consumed by the internal modes of the products, the HCl($v=0,J$) products must experience an impulsive kick to rid the reactants of excess energy. This impulsive kick is expected to excite the HCl products rotationally and is likely to occur in the direction of the C–H bond in the transition state. Unless the transition state rotates significantly, the C–H bond will be on the hemisphere pointing toward the Cl-atom approach. Thus, the impulse release will cause the HCl($v=0$) products to be backward and side scattered and cause the CH_3 radical to rotate preferentially about its C–H bond, which is what we observe experimentally.

The CH_3 product is believed to behave primarily as a spectator during the reaction because of the low degree of methyl radical excitation. Other studies involving reactions of atomic chlorine with overtone excited methane and isotopomers also show that the methyl radical does not participate in the reaction.[13,16,45] Based on the measured spatial anisotropy and energetic constraints, the umbrella bend excited methyl radical products are believed to be formed predomi-

nantly in coincidence with HCl($v=0$) products, not HCl($v=1$) products. Furthermore, it is apparent from the DCS of the $CH_3(\nu_2=1)$ products that these products are formed by a similar mechanism as the HCl($v=0,J$) products as the $CH_3(\nu_2=1)$ scattering distributions are near mirror images of the HCl($v=0,J$) scattering distributions. We postulate that the $CH_3(\nu_2=1)$ products are generated from Cl collisions at low to medium impact parameter and the source of the bend excitation is the transformation of the methyl radical from a pyramidal geometry to a planar geometry in the transition state region.

The above-presented impact parameter model is rooted on the idea that vibrational excitation opens the cone of acceptance by localizing energy along the reaction coordinate and reducing the line-of-centers energy,[48] thereby allowing peripheral reactions.[49–51] The nearly indistinguishable rovibrational distributions and scattering distributions of the Cl $+CH_4(\nu_1)$ and Cl$+CH_4(\nu_3)$ reactions indicate that the reactive mechanisms of these two reactions are similar and suggest that the reactive event involves only a single C–H oscillator. Indeed, rovibrational and scattering distributions from the Cl$+CHD_3(\nu_1)$ reaction,[36] in which there is only one vibrationally excited C–H oscillator, are remarkably similar to the rovibrational distributions and scattering distributions of the Cl$+CH_4(\nu_1)$ and Cl$+CH_4(\nu_3)$ reactions. Thus, a symmetric C–H stretch appears to behave just as an antisymmetric C–H stretch in controlling product internal-state distribution and angular distribution. The relative phases of the other C–H oscillators in CH_4 seem to be inconsequential.

This simple picture is in apparent contradiction with theoretical[21–31] and experimental results[33,34] in which the symmetric stretch is found to be more reactive than the antisymmetric stretch. Our measurements do not necessarily invalidate these previous studies, however, because it is possible for the symmetric stretch to be more reactive than the antisymmetric stretch and for the Cl$+CH_4(\nu_1)$ and Cl $+CH_4(\nu_3)$ reactions to still have identical product rovibrational and scattering distributions. Moreover, our measurements can actually be used to support the conclusions derived from the experiments of Yoon *et al.*[34] Because they performed action spectroscopy on only the 0_0^0 band of the CHD_2 product, one of the uncertainties in their experiment was whether or not the state distributions of the symmetric and antisymmetric stretch excited reactions were the same. Our measurements indicate that their assumption of identical state distributions is most likely valid. Thus, we believe that the initial preparation of the reagents alters the reactivity, but the dynamics leading to product formation follow a common pathway, which could be promoted by vibrational mixing during the collision event.

Yoon *et al.*[34] proposed a vibrationally adiabatic model for the Cl$+CH_4$ reaction similar to the models of Fair *et al.*[32] for the Cl$+H_2O$ reaction and Halonen *et al.*[30] for the reaction of CH_4 on nickel surfaces: the approach of the Cl atom causes the vibrational energy of the CH_4 symmetric and antisymmetric stretches to become localized in the proximal and distal C–H bonds, respectively. As a consequence, the symmetric stretch has more energy along the reaction coordinate, leading to an increased reactivity of the symmetric stretch over the antisymmetric stretch. Although the vibrationally adiabatic model successfully predicts the increased reactivity of the symmetric stretch over the antisymmetric stretch, there are limitations to its predictive abilities. First, the model suggests that excitation of the antisymmetric stretch should not enhance the reactivity at all, in contrast to experimental measurements that estimate the vibrational enhancement factor over the ground state reaction to be $\sim$30 for the Cl$+CH_4(\nu_3)$ reaction.[52] Yoon *et al.* attributed the residual reactivity of the antisymmetric stretch to collision-induced mode-mixing, which was beyond the scope of their model. Our results are consistent with the hypothesis. Second, the model suggests that the symmetric stretch should couple energy more efficiently into HCl product vibration, producing a larger HCl($v=1$):HCl($v=0$) ratio for the Cl $+CH_4(\nu_1)$ reaction. The model also predicts that the CH_3 products from the Cl$+CH_4(\nu_3)$ reaction should be vibrationally excited because the vibrational energy of the antisymmetric stretch is localized into the ''distal'' or nonreactive C–H bonds. In contrast, we observe the same HCl($v=1$):HCl($v=0$) ratio for both the Cl$+CH_4(\nu_1)$ and the Cl $+CH_4(\nu_3)$ reactions, and we do not observe vibrationally excited CH_3 from the Cl$+CH_4(\nu_3)$ reaction. Truhlar and co-workers[28,53] have cautioned previously that the assumption of vibrational adiabaticity may not hold along the entire reaction path. Thus, the initial reactant vibrational motions may not correlate well to the product vibrational motions in the asymptotic region. Another limitation of the vibrational adiabatic model proposed by Yoon *et al.*[34] as well as other theoretical models,[29] is the restriction on the Cl atom to have zero impact parameter and to make a collinear approach to the C–H bond. Based on our DCS measurements, we believe that vibrational excitation opens the cone of acceptance to a large range of impact parameters. Moreover, we believe that greater than 30% of the products, namely the forward scattered HCl($v=1,J$) products, result from collisions at high impact parameter and a T-shaped geometry in the transition state region. The effects of these different reactive geometries are not incorporated in the current theoretical models. Clearly, higher dimensionality models are necessary to fully understand the differences between the effects of the symmetric and antisymmetric stretches on the Cl$+CH_4$ reaction. Although the source of the increased reactivity of the symmetric stretch as compared to the antisymmetric stretch may not be fully established, we find that it does not cause any differences in product state or scattering distributions.

V. CONCLUSION

We have measured rovibrational and state-selected scattering distributions for the HCl and CH_3 products from the Cl$+CH_4(\nu_1)$ and Cl$+CH_4(\nu_3)$ reactions. Detailed comparisons of these quantities show that there is no difference within our resolution and measurement uncertainty between the mechanisms of the Cl$+CH_4(\nu_1)$ and Cl$+CH_4(\nu_3)$ reactions, despite theoretical and experimental results that show the symmetric stretch (ν_1) to be more reactive than the antisymmetric stretch (ν_3). The results presented here suggest that the reactive event involves only a single C–H oscillator

and that vibrational excitation of a C–H stretch increases reactivity by opening the cone of acceptance to allow peripheral reactions. We have presented a model in which the impact parameter governs the state distributions and scattering angle of the products.

Our results represent a counterexample of the mode selectivity observed previously with other vibrationally excited direct reactions. The lack of difference between the dynamical effects of these nearly isoenergetic vibrations on the $Cl+CH_4$ reaction suggest that a symmetric C–H stretch behaves as an antisymmetric C–H stretch in determining product formation. The apparent discrepancies between our results and others dictate that further experimental and theoretical investigations are necessary to fully understand the role that vibrations play in polyatomic reactions.

ACKNOWLEDGMENTS

H.A.B. and J.P.C. thank the National Science Foundation for graduate fellowships. H.A.B. also acknowledges Stanford University for the award of a Stanford Graduate Fellowship. This material is based upon work supported by the National Science Foundation under Grant No. 0242103.

[1] J. C. Polanyi, Acc. Chem. Res. **5**, 161 (1972).
[2] A. Sinha, M. C. Hsiao, and F. F. Crim, J. Chem. Phys. **92**, 6333 (1990).
[3] M. J. Bronikowski, W. R. Simpson, B. Girard, and R. N. Zare, J. Chem. Phys. **95**, 8647 (1991).
[4] A. Sinha, M. C. Hsiao, and F. F. Crim, J. Chem. Phys. **94**, 4928 (1991).
[5] A. Sinha, J. D. Thoemke, and F. F. Crim, J. Chem. Phys. **96**, 372 (1992).
[6] R. B. Metz, J. D. Thoemke, J. M. Pfeiffer, and F. F. Crim, J. Chem. Phys. **99**, 1744 (1993).
[7] M. J. Bronikowski, W. R. Simpson, and R. N. Zare, J. Phys. Chem. **97**, 2204 (1993).
[8] M. J. Bronikowski, W. R. Simpson, and R. N. Zare, J. Phys. Chem. **97**, 2194 (1993).
[9] J. D. Thoemke, J. M. Pfeiffer, R. B. Metz, and F. F. Crim, J. Phys. Chem. **99**, 13748 (1995).
[10] C. Kreher, R. Theinl, and K.-H. Gericke, J. Chem. Phys. **104**, 4481 (1996).
[11] C. Kreher, J. L. Rinnenthal, and K.-H. Gericke, J. Chem. Phys. **108**, 3154 (1998).
[12] J. M. Pfeiffer, E. Woods, R. B. Metz, and F. F. Crim, J. Chem. Phys. **113**, 7982 (2000).
[13] Z. H. Kim, H. A. Bechtel, and R. N. Zare, J. Am. Chem. Soc. **123**, 12714 (2001).
[14] S. Yoon, R. J. Holiday, and F. F. Crim, J. Chem. Phys. **119**, 4755 (2003).
[15] R. D. Beck, P. Maroni, D. C. Papageorgopoulos, T. T. Dang, M. P. Schmid, and T. R. Rizzo, Science **308**, 98 (2003).
[16] H. A. Bechtel, Z. H. Kim, J. P. Camden, and R. N. Zare, J. Chem. Phys. **120**, 791 (2004).
[17] F. F. Crim, J. Phys. Chem. **100**, 12725 (1996).
[18] R. N. Zare, Science **279**, 1875 (1998).
[19] F. F. Crim, Acc. Chem. Res. **32**, 877 (1999).
[20] G. C. Schatz, J. Chem. Phys. **71**, 542 (1979).
[21] G. C. Schatz, M. Colton, and J. Grant, J. Phys. Chem. **88**, 2971 (1984).
[22] D. Wang and J. Bowman, J. Chem. Phys. **96**, 8906 (1992).
[23] D. Wang and J. Bowman, J. Chem. Phys. **101**, 8646 (1994).
[24] D. Zhang and J. Light, J. Chem. Phys. **104**, 4544 (1996).
[25] J. Corchado and J. Espinosa-Garcia, J. Chem. Phys. **105**, 3160 (1996).
[26] J. Espinosa-Garcia and J. C. Corchado, J. Chem. Phys. **105**, 3517 (1996).
[27] J. Espinosa-Garcia and J. Corchado, J. Phys. Chem. **100**, 16561 (1996).
[28] J. C. Corchado, D. G. Truhlar, and J. Espinosa-Garcia, J. Chem. Phys. **112**, 9375 (2000).
[29] J. Palma and D. Clary, Phys. Chem. Chem. Phys. **2**, 4105 (2000).
[30] L. Halonen, S. Bernasek, and D. Nesbitt, J. Chem. Phys. **115**, 5611 (2001).
[31] J. Palma, J. Echave, and D. Clary, Chem. Phys. Lett. **363**, 529 (2002).
[32] J. Fair, D. Schaefer, R. Kosloff, and D. Nesbitt, J. Chem. Phys. **116**, 1406 (2002).
[33] S. Yoon, S. Henton, A. N. Zivkovic, and F. F. Crim, J. Chem. Phys. **116**, 10744 (2002).
[34] S. Yoon, R. J. Holiday, E. L. Silbert, and F. F. Crim, J. Chem. Phys. **119**, 9568 (2003).
[35] J. Palma and D. C. Clary (private communication).
[36] W. R. Simpson, T. P. Rakitzis, S. A. Kandel, A. J. Orr-Ewing, and R. N. Zare, J. Chem. Phys. **103**, 7313 (1995).
[37] R. Atkinson, D. L. Baulch, R. A. Cox, J. R. F. Hampson, J. A. Kerr, and J. Troe, J. Phys. Chem. Ref. Data **21**, 1125 (1992).
[38] W. B. DeMore, S. P. Sander, C. J. Howard, A. R. Ravishankara, D. M. Golden, C. E. Kolb, R. F. Hampson, M. J. Kurylo, and M. J. Molina, Jet Propulsion Laboratory, Pasadena, CA, 1997.
[39] W. R. Simpson, A. J. Orr-Ewing, T. P. Rakitzis, S. A. Kandel, and R. N. Zare, J. Chem. Phys. **103**, 7299 (1995).
[40] W. C. Wiley and I. H. McLaren, Rev. Sci. Instrum. **26**, 1150 (1955).
[41] P. C. Samartzis, B. Bakker, T. P. Rakitzis, D. H. Parker, and T. N. Kitsopoulos, J. Chem. Phys. **110**, 5201 (1999).
[42] A. Yokoyama and T. Takayanagi, Chem. Phys. Lett. **307**, 48 (1999).
[43] E. A. Rohlfing, D. W. Chandler, and D. H. Parker, J. Chem. Phys. **87**, 5229 (1987).
[44] J. W. Hudgens, T. G. DiGiuseppe, and M. C. Lin, J. Chem. Phys. **79**, 571 (1983).
[45] Z. H. Kim, H. A. Bechtel, and R. N. Zare, J. Chem. Phys. **117**, 3232 (2002).
[46] R. O. Loo, H.-P. Haerri, G. E. Hall, and P. L. Houston, J. Chem. Phys. **90**, 4222 (1989).
[47] D. W. Chandler, J. W. Thoman Jr., M. H. M. Janssen, and D. H. Parker, Chem. Phys. Lett. **156**, 151 (1989).
[48] R. D. Levine and R. B. Bernstein, *Molecular Reaction Dynamics and Chemical Reactivity* (Oxford University Press, New York, 1987).
[49] P. M. Aker and J. J. Valentini, Isr. J. Chem. **30**, 157 (1990).
[50] M. Ben-Nun, M. Brouard, J. P. Simons, and R. D. Levine, Chem. Phys. Lett. **210**, 423 (1993).
[51] X. Wang, M. Ben-Nun, and R. D. Levine, Chem. Phys. **197**, 1 (1995).
[52] W. R. Simpson, T. P. Rakitzis, S. A. Kandel, T. LevOn, and R. N. Zare, J. Phys. Chem. **100**, 7938 (1996).
[53] B. C. Garrett, D. G. Truhlar, J. M. Bowman, and A. F. Wagner, J. Chem. Phys. **90**, 4305 (1986).
[54] W. J. van der Zande, R. Zhang, R. N. Zare, K. G. McKendrick, and J. J. Valentini, J. Phys. Chem. **95**, 8205 (1991).